Assessing the activity of Ni clusters supported on TiC(001) towards CO_2 and H_2 dissociation

Pablo Lozano-Reis,[1] Hector Prats[2], Ramón Sayós,[1] José A. Rodriguez,[3] Francesc Illas[1]

1) Departament de Ciència de Materials i Química Física & Institut de Química Teòrica i Computacional (IQTCUB), Universitat de Barcelona, C. Martí i Franquès 1, 08028 Barcelona, Spain

2) Department of Chemical Engineering, University College London, Roberts Building, Torrington Place, London WC1E 7JE, UK

3) Department of Chemistry, Brookhaven National Laboratory, Upton, New York, 11973-5000, U.S.A.

Abstract

Small Ni particles supported on TiC(001) have been shown to display a very high activity for the catalytic hydrogenation of CO_2 but the underlying chemistry is, to a large extent, unknown. Here, by means of periodic density functional theory (DFT) calculations with the BEEF-vdW functional, we explore the adsorption and subsequent dissociation of CO_2 and H_2 on several Ni_n clusters (n = 4, 9, 13 and 16) supported on TiC(001) and compare the results to those obtained for the bare Ni(111) and TiC(001) surfaces, using exactly the same computational approach. The calculations reveal that the Ni_n/TiC system exhibits stronger adsorption energies and lower dissociation energy barriers for CO_2 and H_2 than the bare Ni(111) and TiC(001) surfaces. This is in line with the experimental finding evidencing that the Ni/TiC system has a catalytic activity higher than that of the separated Ni and TiC constituents. In addition, the calculated results show that supported two-dimensional (2D) clusters adsorb CO_2 and H_2 stronger than the supported three-dimensional (3D) clusters and also 2D clusters exhibit lower energy barrier for CO_2 dissociation. Within the 2D supported clusters, larger particles feature slightly stronger adsorption energies and lower CO_2 dissociation energy barriers. Finally, H_2 dissociation proceeds with a very low energy barrier on all the studied models which makes these novel systems potential good candidates for hydrogenation reactions.

KEYWORDS: CO_2 dissociation, H_2 dissociation, nickel clusters, titanium carbide, supported clusters activity, density functional theory calculations.

1. INTRODUCTION

Excessive emissions of greenhouse gases are producing a devastating effect on the Earth environment leading to phenomena such as the global warming with direct impact on the overall climate system. Among the different greenhouse gases, carbon dioxide (CO_2) is the major contributor to global warming and sea acidification.[1,2] The increase of atmospheric CO_2 is directly associated to the use of carbon-rich fossil fuels for covering the ever-growing world energy demand. Unfortunately, satisfying the whole current world energy requirements with green energies is still remote[3,4] and significant efforts are being addressed toward the CO_2 catalytic chemical conversion. This strategy, involves simultaneously reducing the environmental impact related to CO_2 emissions and generating energy carriers, thus creating a cyclic energy economy. In the last decades, CO_2 hydrogenation has gained interest for generating new value-added chemicals of industrial significance. Among the different chemicals of industrial interest, CO, methane, methanol and formaldehyde are the most investigated options[5-8] and all require appropriate active and selective catalysts.

The most common heterogeneous catalysts used in industrial applications consist of small to medium size metallic nanoparticles anchored on some type of support, usually an oxide or sulphide.[9] The nature of both, metal and support, controls the catalytic activity and, more importantly, the selectivity towards a specific product. Normally, precious metals like Pd and Pt are highly active, but they are scarce and expensive. Therefore, metals that could be active, abundant and cheap attract considerable attention. In that sense, Ni-based catalysts are widely used for the CO_2 hydrogenation reaction due to its relatively high activity and low cost compared to noble metals.[10-17] In these catalysts, nickel nanoparticles are often supported over different metal oxides although transition metal carbides (TMCs) were also proposed as supports,[18-20] the resulting systems exhibiting high activity and selectivity. The enhanced activity was attributed to the polarization that the TMC surface provokes on the supported particle electronic density.[21] This type of positive interaction between the metal cluster and the TMC support is different from the so-called strong metal support interactions (SMSI) introduced by Tauster, that are detrimental to the catalytic activity.[22-24] Indeed, there is increasing evidence of a possible positive active role of the support and it is now clear that metal-support interactions in many cases can be used to tune a specific activity and selectivity.[25] For instance, Klyushin et al.[26] evidenced the benefits of metal-support interactions for the CO oxidation reaction catalysed by Au nanoparticles supported on TiO_2. Similarly, Bruix et al.[27] showed an activity enhancement for the water gas shift reaction (WGSR) on Pt clusters anchored over a ceria support that was due to metal-support interactions. Moreover, in a recent study, Prats et al.[28] showed the interplay between the metal and the support for the WGSR on Au clusters supported on molybdenum carbide using a multiscale approach. Clearly, catalysis design can benefit from the use of metal-support interactions that open new opportunities for the generation of tailor-made materials.

Coming back to the case of CO_2 activation, experiments under well controlled conditions showed that Ni clusters supported on titanium carbide (TiC) exhibit a high activity towards CO_2 hydrogenation[20] with a

noted selectivity towards CO production, although the underlying chemistry is essentially unknown. In part, this is due to the complex network of reactions that are involved in this apparently simple reaction where direct dissociation of CO_2 and H_2 competes with hydrogen-assisted CO_2 dissociation to CO and COOH formation, that eventually leads to a small amount of methanol. On extended surfaces of nickel, the products of the hydrogenation of CO_2 can be CO, methanol, methane, other light alkanes, and coke. Thus, the high selectivity seen on Ni/TiC(001) for the production of CO is remarkable.[20]

Recent work has shown that TiC(001) and TiC powders can storage large amounts of hydrogen that are available for any hydrogenation process.[29] Thus, in Ni/TiC(001), one has a catalyst in which the properties of the carbide and metal-support interactions may be responsible for the high selectivity seen during CO_2 hydrogenation.[20] Furthermore, in this system, the reactivity also depends on the size of the supported metal particle, being small two-dimensional (2D) supported clusters more active than larger three-dimensional (3D) clusters.[20] This is likely due to differences in the electronic distribution of the supported 2D and 3D Ni clusters induced by the TiC support. Precisely, a recent study has shown that Ni clusters bind stronger over TiC than over different reducible and non-reducible metal oxides.[30] This study also revealed that 3D clusters should be easier to form and are more stable, which can be beneficial for catalysis, provided the morphology of the supported clusters can be controlled. The clear influence of the particle size and morphology further complicates the situation and calls for modelling studies where the different effects can be studied separately. To contribute to disentangle this problem, we have studied the size and morphology effect of supported nickel clusters on the adsorption and dissociation of CO_2 and H_2. This is a necessary step before selecting an appropriate catalytic model to thoroughly study the CO_2 hydrogenation reaction by a multiscale approach.

2. COMPUTATIONAL METHODS AND MATERIAL MODELS

The adsorption and dissociation of CO_2 and H_2 on a series of models representing a variety of Ni clusters supported on TiC (*vide infra*) were studied by means of density functional theory (DFT)-based calculations using periodic models. All calculations described in the present work were carried out by means of the Vienna Ab Initio Simulation Package (VASP) code[31-33] where the valence electron density is expanded in a plane wave basis set, as indicated below, while the effect of the core electrons on the valence electron density is represented by the projector augmented wave (PAW) method.[34] Spin-polarization has been considered for all the systems containing Ni, in order to account for its magnetic properties arising from its incomplete occupation of the 3d shell. All DFT calculations were carried out using the nonlocal BEEF-vdW exchange correlation functional[35] that includes dispersion effects. The reason for this particular choice comes from several benchmark studies showing that it provides better agreement with available experimental data than other commonly used functionals.[35-37]

The different systems representing Ni clusters supported on the TiC(001) surface were modelled by a (N×M) supercell containing four TiC atomic layers plus the Ni_4, Ni_9, Ni_{13} and Ni_{16} clusters as shown in Figure 1. In these systems, we change the number of atoms in the cluster and consider configurations in which all the

nickel atoms are in contact with the carbide substrate (maximizing metal-support interactions) or have a 3D configuration where some of its atoms do not touch the support. For comparison, the interaction of CO_2 and H_2 with the Ni(111) and TiC(001) surfaces were also considered with data calculated here using the same computational approach and compared to previous values in the literature.[20,38] Regarding the models for the supported clusters, one should be aware that several near degenerate structural isomers may be present, especially at operating conditions.[39,40] However, the focus of the present work is on the effect of cluster size and shape (2D versus 3D atomic structures) rather than a complete study of the reactivity of different isomers for each supported cluster. This will shed light on important aspects of a complex reaction network by guiding appropriate catalysts models that, even if not perfect, are realistic enough to provide physically meaningful insights about the molecular process by subsequent multiscale simulations.

The size of the supercell was large enough to avoid spurious interactions between periodically repeated species. Similarly, a vacuum width of at least 12 Å was used to minimize spurious interactions between periodically repeated slabs in the vertical direction. In all calculations at least the outmost TiC atomic layer, the nickel cluster and the adsorbed species were allowed to fully relax, while the other TiC layers were fixed to provide a bulk environment to the surface region. A cutoff energy of 415 eV was set for the plane wave expansion while the Monkhorst-Pack[41] *k*-point mesh was varied depending on the surface model used. The specific values used for each surface model are summarized in Table S1 in the supporting information (SI). The electronic energy convergence criterion was set to 10^{-5} eV, while atomic positions were allowed to relax until the forces acting on the atoms were smaller than 0.01 eV $Å^{-1}$. Note that for calculations in which convergence problems have aroused, we have ensured that the electronic energy does not vary more than 10^{-3} eV.

Transition states (TS) structures were located using the climbing-image nudged elastic band method (CI-NEB).[42,43] The initial guesses for the employed intermediate images were generated using the image dependent pair potential procedure[44] as implemented in the Atomic Simulation Environment (ASE) package.[45] Vibrational frequency analysis was carried out to ensure that all TS have only one imaginary frequency whereas for adsorbed species all frequencies were positive thus corresponding to real minima on the potential energy surface. The calculated frequencies were also used to compute the zero-point energy (ZPE) contribution to the energy of all adsorbed species. The energy of gas-phase molecules was calculated by placing a single molecule in a box of dimensions $9 \times 10 \times 11$ $Å^3$ and considering the Γ point only. Then, the adsorption energy of the considered i species was calculated as follows:

$$E_{ads,i} = E_{i,slab} - E_{slab} - E_{i,g} \quad (1)$$

where $E_{i,slab}$ is the energy of the i species adsorbed over the surface, E_{slab} is the energy of the relaxed pristine surface and $E_{i,g}$ is the i gas-phase energy. With this definition, favourable adsorption corresponds to negative $E_{ads,i}$ values. Reaction energies (ΔE_r) and energy barriers ($\Delta E^{\neq}$) were calculated as:

$$\Delta E_r = E_{FS} - E_{IS} \quad (2)$$

$$\Delta E^{\neq} = E_{TS} - E_{IS} \quad (3)$$

where E_{IS}, E_{FS} and E_{TS} are the total energy of the initial, final and transition states, respectively. Note that for the final states, the co-adsorbed configuration (i.e., CO + O or H + H) was always considered. Unless otherwise specified, all energy values reported in the present work include the ZPE contribution.

3. RESULTS AND DISCUSSION

3.1 CO_2 and H_2 adsorption on Ni_n/TiC models. The adsorption energies for CO_2 and H_2 on the different sites of the four Ni_n/TiC different model systems as well as on bare TiC(001) and Ni(111) are shown in Table 1; the most stable configurations are schematically displayed in Figure 2. As shown in Figure 2, a similar pattern emerges for both CO_2 and H_2 adsorbed molecules. On the bare TiC(001) and Ni(111) surfaces, the CO_2 adsorption energies calculated with the BEEF-vdW functional are of -0.58 eV and -0.15 eV, indicating chemisorption and physisorption, respectively. It is known that CO_2 interacts weakly with Ni(111) and with other surfaces of late transition metals.[46,47] For CO_2 adsorption on TiC(001) the reported BEEF-vdW value is close to the PBE ones reported by Kunkel et al.[48] (-0.57 eV) and by López et al.[49,50] (-0.61) and slightly smaller than the PBE-D3 value reported by the same authors (-0.83 eV and -0.85 eV, respectively). The small difference is clearly due to the different treatment of dispersion in the BEEF-vdW and PBE-D3 approaches, the latter known to overestimate the adsorption energy. Apart from this small discrepancy, all studies point to formation of a C_{surf}-CO_2 bond giving an adsorption configuration in which the molecule is activated with a concomitant increase of the C-O bond lengths and appearance of significant O-C-O bending (see Table 1). On the other hand, H_2 has a similar interaction with both TiC(001) and Ni(111), being physisorbed on both surfaces.

For the Ni cluster supported on TiC(001), the strong metal-support interaction[30] generates a charge redistribution over the Ni atoms that results in much larger adsorption energies for both CO_2 and H_2 (see Figure 2). On the Ni_n/TiC systems, adsorption induces a strong activation of both molecules evidenced by increased bond lengths and, in the case of CO_2, a large deviation from linearity (see Table 1). As a curiosity, C-O and H-H bond lengths nicely correlate with the CO_2 and H_2 adsorption energies, respectively; so, the largest the bond length the largest the adsorption energy, as shown in Figure 3. Regarding the effect of the supported morphology, those clusters with a 2D atomic structure adsorb CO_2 and H_2 strongly than the 3D one. The reason for this behaviour is simply that the Ni atoms in the 2D clusters are more affected by the underlying TiC support than those of the supported 3D clusters where there are Ni atoms that are not in direct contact with the support and, consequently, much less affected. This is a general trend already observed for other metallic particles supported on TMCs.[21,51] Within 2D clusters, adsorption energies slightly increase with particle size, which can be attributed to the lower energy penalty for structure reconstruction upon adsorption on Ni_{16}/TiC compared to Ni_4/TiC and Ni_9/TiC.[21] Interestingly, the topmost hollow site of Ni_{13}/TiC does not

adsorb CO_2 nor H_2, as this site closely resembles the four-fold hollow site of the Ni(100) surface that is known to interact poorly with CO_2, but it can interact significantly with H_2.[52]

To have a better perspective of the different interactions involved in the H_2 and CO_2 adsorption with the different Ni_n cluster supported on TiC, it is interesting to compare with other studies of similar systems either involving TiC(001) surfaces doped with metals[49,50] or other supported metals on TiC(001).[20,53,54] A comparison with these previous works shows that Ni_n/TiC(001) systems are really attractive as they interact stronger with H_2 and CO_2. For instance, for H_2 adsorption, Florez et al.[53] reported adsorption energy values of 0.01 and -0.04 eV for the Au_4/TiC and Au_9/TiC systems, respectively. These values were obtained using a different but quite similar functional —PW91 without including dispersion— but, in any case, are significantly smaller than the BEEF-vdW calculated values for the Ni_4/TiC and Ni_9/TiC systems (-0.34 and -0.35 eV, respectively). Note that Florez et al.[53] also reported an H_2 adsorption energy of -0.48 eV on the bare TiC(001) surface, which is larger than the present calculated value (-0.01 eV). An analysis of the involved structures shows that the value reported by Florez et al.[53] corresponds to a nearly dissociated structure with a H-H distance of 1.73 Å, as specified by the authors, whereas the present calculations clearly find a physisorbed H_2 molecule. Clearly, the lack of dispersion in the PW91 functional used by Florez et al.[53] is the reason why the physisorbed species was not detected in the calculations. In a subsequent work, Gomez et al.[54] studied the adsorption of H_2 on a series of M_4/TiC systems (M = Pd, Pt, Cu, Ag and Au). They used the same PW91 functional, again without including dispersion, and found an almost negligible H_2 adsorption energy on the Cu_4/TiC, Ag_4/TiC and Au_4/TiC systems. Oppositely, they found a stronger adsorption energy for the Pd_4/TiC and Pt_4/TiC systems (-0.70 and -0.87 eV, respectively). In spite of the use of a density functional neglecting dispersion, the trends are physically sound and can be safely compared to the present BEEF-vdW values. The present value for the H_2 adsorption energy on Ni_4/TiC of -0.34 eV is clearly in between the values for coinage and Pt-group metals. Moreover, both Pd_4/TiC and Pt_4/TiC exhibit a rather large energy barrier for dissociation (*vide infra*), which makes Ni_4/TiC more attractive for H_2 dissociation as discussed more in detail in the next section.

Regarding CO_2 adsorption, as mentioned above, it is known that the molecule interacts weakly with Ni(111) and with other surfaces of late transition metals.[46,47] It is interesting to compare to the results reported by López et al.[49,50] who studied the effect of doping the TiC(001) surface with different kinds of metals. In particular, these authors first considered the situation where one surface Ti atom is replaced by another transition metal atom chosen from the list of those that are commonly present in TMCs such as Zr, Hf, V, Nb, Mo, Cr, Ta and W. They found that the highest CO_2 adsorption energy corresponded to the Hf and Zr doped systems, with PBE adsorption energies of -0.96 and -0.93 eV, respectively. In both cases, CO_2 adsorbs via a C_{surf}-CO_2 bond with one of the oxygen atoms pointing to the dopant. In a following study, these authors increased the set of doping atoms so as to include Mg, Ca, Sr, Al, Ga, In, Si, Sn, Pd, Pt, Rh, Ir, La and Ce, and found that, among all dopants studied, the Sr and Ce doped systems exhibited the largest adsorption energy. However, they also found significant differences in the bonding mechanism; CO_2 interacts directly with Ce

dopant resulting in a PBE adsorption energy of -1.10 eV but in the case of Sr the bonding mode does not involve such direct interaction and the reported PBE adsorption energy was -1.22 eV. However, these values are still slightly smaller than those of the 2D Ni_n/TiC systems of -1.37, -1.41 and -1.49 eV for the Ni_4/TiC, Ni_9/TiC and Ni_{16}/TiC systems, respectively, although these include dispersion through the BEEF-vdW functional. Note that in the present calculations the bonding mode implies a clear direct interaction between the CO_2 molecule and the Ni atoms of the nickel clusters. Finally, Rodriguez et al.[20] reported CO_2 adsorption energies of -1.11, -0.59, -0.68 and -0.37 eV over Cu_4/TiC, Au_4/TiC, Cu_9/TiC and Au_9/TiC, respectively, also lower than 2D Ni_n/TiC systems. Even if these values have been obtained with the PW91 functional and, hence, neglect dispersion, it is clear that the Ni clusters supported on TiC are more active to adsorb CO_2 than those of Cu and Au on the same support. It is also worth noting that for the 3D coinage clusters supported on TiC, the interaction of CO_2 with the uppermost layer was negligible as we have observed for Ni_{13}/TiC. Note that previous studies do not include the ZPE contribution term although its contribution to the adsorption energy is of the order of 0.02 eV or less.

3.2. CO_2 and H_2 dissociation on Ni_n/TiC models. The dissociation of CO_2 and H_2 on the present models is rather complex since both adsorbates interact with a rather similar strength on different sites. Thus, we have considered all possible reaction pathways, which are listed in Table S2 in the SI. Table 2 reports the reaction energies and energy barriers for the pathways exhibiting the lowest energy barrier. The highest dissociation energy barriers for both CO_2 and H_2 correspond to the bare TiC(001) and Ni(111) surfaces with Ni(111) predicted to be slightly more active than TiC(001) for CO_2 and H_2 dissociation. Note that Ni(111) surface activity will be limited by the weak CO_2 and H_2 adsorption, in agreement with experimental trends.[47] Likewise, one must point out that, during the hydrogenation process, the dissociation of the CO_2 molecule can occur either spontaneously or assisted by hydrogen adatoms arising from a previous H_2 dissociation step. These constitute the initial steps of a complex reaction network (see Ref. 38) ultimately determining the selectivity of the process with the possible products being CO, methanol, CH_4 or other light alkanes, and coke. Therefore, to better understand the underlying chemistry, it is convenient to focus first on the adsorption and dissociation of CO_2 and H_2, and this is precisely the aim of the present work.

For the Ni_n/TiC models, the strong metal-support interactions result in moderately low energy barriers for CO_2 direct dissociation with values in the 0.35−0.83 eV range. Moreover, the process is clearly favoured over the 2D supported clusters and, as these adsorb CO_2 stronger, they are suitable candidates for CO_2 conversion. Note also that CO_2 dissociates with similar energy barrier on all the considered different sites of the 2D supported clusters, but this is not the case of 3D clusters (see Table S2 in the SI). Results in Table 2 also indicate that, for the 2D clusters, the CO_2 dissociation energy barrier slightly decreases with cluster size. These minor differences are also observed for the adsorption strength and are rationalized as a smaller reorganization of the supported cluster atomic structure in the largest ones. The energy barriers are even smaller for H_2 dissociation with values as low as 0.02−0.11 eV. Contrarily to what is observed for H_2 adsorption, there is no clear trend relating the Ni_n/TiC atomic structure and the corresponding energy barrier

for H_2 dissociation. However, 2D clusters emerge as excellent candidates for hydrogenation reactions given their very low energy barriers and rather strong H_2 adsorption. Note that the H_2 dissociation mechanism on all supported clusters is very similarly irrespectively on the adsorption site (see Table S2 in the SI). As a final remark, one should mention that the good H_2 dissociation capacity and the ability of TiC(001) to pack large coverages of hydrogen, makes Ni_n/TiC systems really attractive for hydrogenation reactions. Therefore, under regular pressures of H_2, H atoms could migrate from Ni_n clusters to the TiC(001) surface, producing a large H reservoir that could be useful for hydrogenation reactions.

It is interesting to compare the present results with other studies for different metal clusters on the same support.[20,53,54] Clearly, the Ni_n/TiC(001) systems are more attractive for CO_2 hydrogenation as the small energy barrier for H_2 dissociation is accompanied by a rather strong CO_2 adsorption although a systematic study is needed involving all possible intermediates, typically COOH and HCOO, and the subsequent evolution either to CO or methanol. This study is out of the scope of the present work but will be the focus of future studies. Regarding the comparison to previous works, Florez et al.[53] studied the H_2 dissociation reaction over Au_4, Au_9 and Au_{13} clusters supported on TiC(001) surface and considered also the pristine TiC(001) surface. They used the PW91 exchange-correlation functional and did not include dispersion meaning that, as for many of the preceding discussions, a meaningful comparison should focus on trends rather than absolute values. Similar to the present results for the 2D supported Ni clusters, H_2 dissociation on the 2D supported Au cluster was found to involve very small energy barriers (0.08 and 0.20 eV for Au_4/TiC and Au_9/TiC, respectively). However, for the 3D Au_{13}/TiC system the energy barrier was found to be much higher than that reported here for Ni_{13}/TiC; 0.99 and 0.11 eV, respectively. Therefore, while both 2D Au and Ni clusters anchored over TiC(001) are very attractive for hydrogenation reactions, Ni_n/TiC appears as a more robust candidate because, in practice, a control of the supported cluster morphology can be extremely challenging and, at high metal coverage, 3D clusters become predominant. It is also interesting to compare the present results with those reported by Gomez et al.[54] for the catalytic activity of M_4/TiC (M = Pd, Pt, Cu, Ag and Au) systems towards H_2 dissociation. Their calculations with the PW91 functional found that the H_2 dissociation energy barrier follows the order Pt > Ag > Pd > Cu > Au; again, the absolute values of 1.16, 0.79, 0.53, 0.37 and 0.08 eV, respectively, should not be compared while the trend is for sure meaningful. Thus, among the different M_4 supported clusters studied, Ni_4/TiC and Au_4/TiC exhibit the lowest energy barriers. Concerning CO_2 dissociation, Rodriguez et al.[20] reported a PW91 dissociation energy barrier of 0.81 eV on Cu_4/TiC, which is significantly larger than our BEEF-vdW calculated value of 0.55 eV for Ni_4/TiC. In addition, the adsorption energy of CO_2 on Cu_4/TiC (-1.11) is smaller than on Ni_4/TiC (-1.37 eV). Therefore, Ni_n/TiC systems are predicted to be more active that the Cu_n/TiC and Au_n/TiC systems, which nicely agrees with experimental findings.[20]

CONCLUSIONS

The adsorption and subsequent dissociation of CO_2 and H_2 has been studied for a series of 2D and 3D Ni clusters supported on TiC(001), using suitable periodic models and density functional calculations with the BEEF-vdW exchange-correlation functional including dispersion. The 2D clusters contained 4, 9, and 16 Ni atoms whereas Ni_{13} was selected as representative of the 3D ones. For compassion, bare Ni(111) and TiC(001) surfaces were also considered so that all systems have been studied using exactly the same computational approach. The present study allowed us to reach firm conclusions regarding the effect of the cluster size and of metal-support interactions on the catalytic activity of these novel systems.

The present systematic study shows that both CO_2 and H_2 molecules adsorb in general on Ni_n/TiC(001) stronger than on the bare Ni(111) and TiC(001) surfaces, with dissociation energy barriers that are quite low and smaller than for these two extended surfaces. The present results also indicate that the 2D supported clusters adsorb CO_2 and H_2 stronger and dissociate CO_2 easier than the 3D supported clusters. In all studied Ni_n/TiC(001) models, H_2 dissociates with very low energy barriers with no clear trend. We also show that, for the supported 2D clusters, the larger particles feature slightly stronger adsorption energies and lower CO_2 energy barriers, although the differences are minimal. These minor differences are attributed to the fact that the larger clusters exhibit a smaller atomic reorganization when the molecule adsorbs and, eventually, dissociates. A comparison with previous studies on similar systems shows that Ni_n/TiC(001) systems are more attractive for CO_2 and H_2 dissociation than metal-doped TiC(001) surfaces and other metal clusters supported on TiC(001).

ACKNOWLEDGMENTS

The research at the *Universitat de Barcelona* has been supported by the Spanish Ministry of Science, Innovation and Universities (MICIUN) through grants RTI2018-094757-B-I00, RTI2018-095460-B-I00, MCIU/AEI/FEDER, UE and MDM-2017-0767, and in part, by the *Generalitat de Catalunya* (grant 2017SGR13). The work carried out at the Brookhaven National Laboratory (BNL) was supported by the U.S. Department of Energy, Office of Science and Office of Basic Energy Sciences under contract No. DE-SC0012704. P. L-R. acknowledges MICIUN for a predoctoral FPU18/02313 grant. Computational resources provided by *Consorci de Serveis Universitaris de Catalunya* (CSUC, former CESCA) with financial support from *Universitat de Barcelona* and *Red Española de Supercomputación* (grants QS-2020-1-0003 and QS-2020-2-0009) are gratefully acknowledged.

ASSOCIATED CONTENT

Supporting Information

The supporting information is available free of charge at DOI

Information about specific values used for each of the studied surface models (Sec. S1), the CO_2 and H_2 dissociation energy barriers and the initial, final and transition state structures of each reaction (Sec. S2). Optimized structures (i.e., VASP CONTCAR files) of all relevant structure have been also made available on a public GitHub repository: https://github.com/plozanore/Nin-TiC_CO2_H2_dissociation

AUTHOR INFORMATION

Corresponding Author

Francesc Illas - *Departament de Ciència de Materials i Química Física & Institut de Química Teòrica i Computacional (IQTCUB), Universitat de Barcelona, C. Martí i Franquès 1, 08028 Barcelona, Spain.*

Authors

Pablo Lozano-Reis - *Departament de Ciència de Materials i Química Física & Institut de Química Teòrica i Computacional (IQTCUB), Universitat de Barcelona, C. Martí i Franquès 1, 08028 Barcelona, Spain.*

Hector Prats - *Department of Chemical Engineering, University College London, Roberts Building, Torrington Place, London WC1E 7JE, UK*

Ramón Sayós - *Departament de Ciència de Materials i Química Física & Institut de Química Teòrica i Computacional (IQTCUB), Universitat de Barcelona, C. Martí i Franquès 1, 08028 Barcelona, Spain.*

José A. Rodriguez - *Department of Chemistry, Brookhaven National Laboratory, Upton, New York, 11973-5000, U.S.A.*

Notes

There are no conflicts of interest to declare.

Table 1. CO_2 and H_2 adsorption energies (including the ZPE term), C-O bond lengths (d_{C-O}), H-H bond lengths (d_{H-H}) and O-C-O bond angles (θ_{O-C-O}), for the most stable adsorbed sites for H_2 and CO_2 over the different surface models. Note that except in Ni_{13}/TiC(001), the Ni supported clusters have a 2D atomic structure.

CO_2				
Model	site	E_{ads} / eV	d_{C-O} / Å	θ_{O-C-O} / º
Ni(111) [a]	tNi	-0.15	1.18, 1.18	180
TiC(001)	tC	-0.58	1.29, 1.29	128
Ni_4/TiC(001)	hNi	-1.37	1.35, 1.28	122
Ni_9/TiC(001)	hNi_1	-1.36	1.36, 1.29	119
Ni_9/TiC(001)	hNi_2	-1.41	1.36, 1.29	119
Ni_{13}/TiC(001)	tNi_2	-0.47	1.28, 1.28	130
Ni_{13}/TiC(001)	tNi_3	-0.48	1.24, 1.26	138
Ni_{16}/TiC(001)	hNi_1	-1.49	1.36, 1.29	117
Ni_{16}/TiC(001)	hNi_2	-1.45	1.37, 1.29	118
Ni_{16}/TiC(001)	hNi_3	-1.45	1.35, 1.28	120

H_2			
Cluster	site	E_{ads} / eV	d_{H-H} / Å
Ni(111) [a]	bNi	-0.02	0.74
TiC(001)	tM	-0.01	0.74
TiC(001)	tC	-0.01	0.74
Ni_4/TiC(001)	tNi	-0.34	0.83
Ni_9/TiC(001)	tNi_1	-0.30	0.86
Ni_9/TiC(001)	tNi_2	-0.35	0.85
Ni_9/TiC(001)	tNi_3	-0.33	0.83
Ni_{13}/TiC(001)	tNi_2	-0.01	0.82
Ni_{13}/TiC(001)	tNi_3	-0.12	0.82
Ni_{13}/TiC(001)	tNi_1	-0.12	0.83
Ni_{16}/TiC(001)	tNi_1	-0.40	0.84
Ni_{16}/TiC(001)	tNi_2	-0.40	0.84
Ni_{16}/TiC(001)	tNi_3	-0.42	0.83

[a] The Ni(111) values were taken from ref 38.

Table 2. CO_2 and H_2 reaction energy ($\Delta E_{r,0}$) and forward and reverse energy barriers ($\Delta E^{\neq}_{fw,0}$ and $\Delta E^{\neq}_{rev,0}$, respectively) over the most probable sites for reaction of the different considered Ni_n/TiC models with Ni(111) and TiC(001) included for comparison. Note that except Ni_{13}/TiC(001), the Ni supported clusters have a 2D atomic structure. All energy values were obtained with the BEEF-vdW functional and include the ZPE contribution

.

CO_2				
Model	Reaction	$\Delta E_{r,0}$ / eV	$\Delta E^{\neq}_{fw,0}$ / eV	$\Delta E^{\neq}_{rev,0}$ / eV
Ni_4/TiC(001)	$CO_{2,hNi} \rightleftharpoons CO_{hNi} + O_{tTi1}$	0.03	0.55	0.52
Ni_9/TiC(001)	$CO_{2,hNi} \rightleftharpoons CO_{hNi} + O_{tTi1}$	0.25	0.52	0.27
Ni_{13}/TiC(001)	$CO_{2,tNi2} \rightleftharpoons CO_{tNi2} + O_{tTi1}$	-0.39	0.83	1.22
Ni_{16}/TiC(001)	$CO_{2,hNi1} \rightleftharpoons CO_{hNi1} + O_{hNi2}$	-0.68	0.35	1.03
Ni(111)	$CO_{2,top} \rightleftharpoons CO_{hcp} + O_{fcc}$	-0.57	0.86	1.43
TiC(001)	$CO_{2,tC} \rightleftharpoons CO_{tC} + O_{hMMC}$	-0.06	1.03	1.08
H_2				
Model	Reaction	$\Delta E_{r,0}$ / eV	$\Delta E^{\neq}_{fw,0}$ / eV	$\Delta E^{\neq}_{rev,0}$ / eV
Ni_4/TiC(001)	$H_{2,tNi} \rightleftharpoons H_{bNi} + H_{bNi}$	-0.60	0.08	0.68
Ni_9/TiC(001)	$H_{2,tNi1} \rightleftharpoons H_{hNi} + H_{hNi}$	-0.95	0.02	0.97
Ni_{13}/TiC(001)	$H_{2,tNi1} \rightleftharpoons H_{tNi1} + H_{tNi3}$	-0.51	0.11	0.62
Ni_{16}/TiC(001)	$H_{2,tNi3} \rightleftharpoons H_{bNi4} + H_{bNi4}$	-0.44	0.07	0.52
Ni(111)	$H_{2,bNi} \rightleftharpoons H_{fcc} + H_{hcp}$	-0.31	0.28	0.59
TiC(001)	$H_{2\,tM} \rightleftharpoons H_{tC} + H_{tC}$ [a]	-0.50	1.07	1.57

[a] Note that this process occurs in two steps, as shown in Ref. 55. Thus, the energy barrier is calculated with respect to the TS with the highest energy. See Table S2 in the SI for information about the energetics of each of the two-steps.

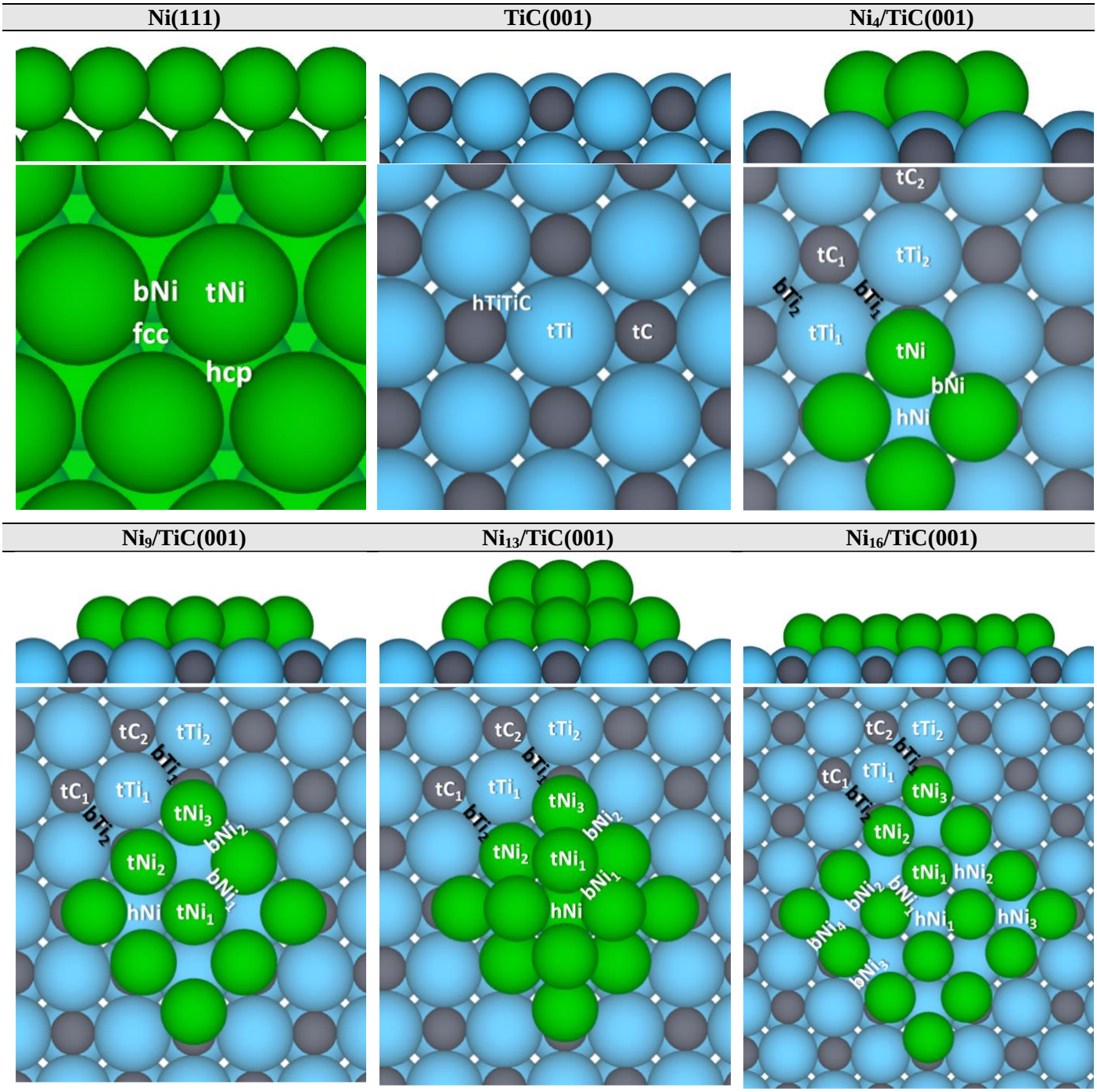

Figure 1. Side and top views of the 6 different surface models studied. Top view contains the label of the different considered adsorption sites. Light blue, grey and green colours are used for titanium, carbon and nickel, respectively.

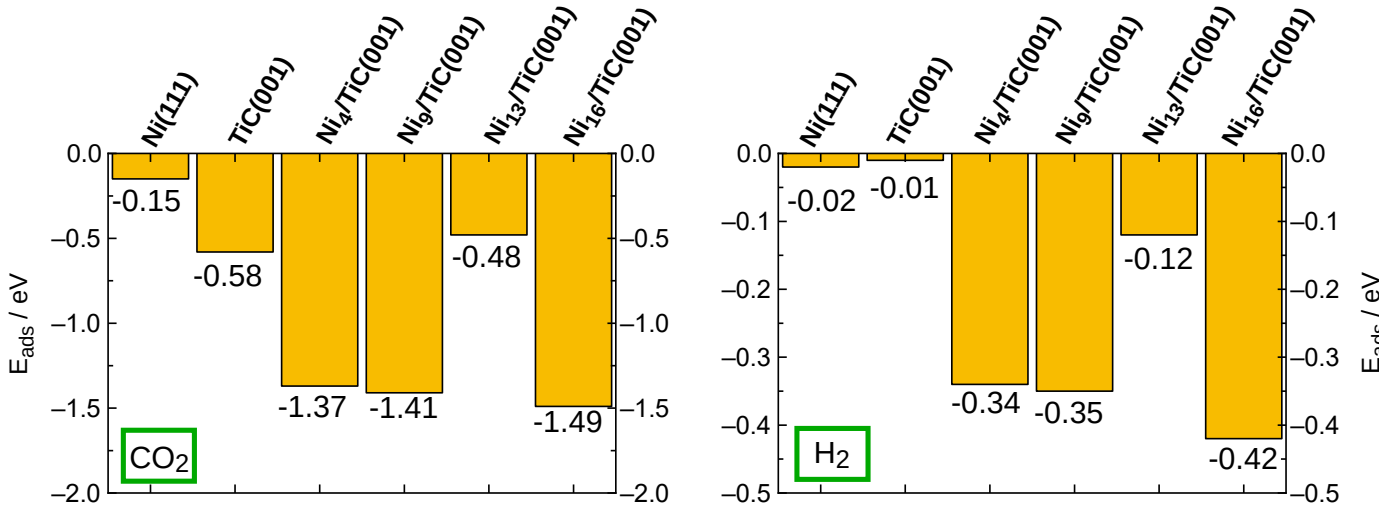

Figure 2. H_2 and CO_2 adsorption energies over different surface models. The ZPE term is included. The adsorption energies on Ni(111) were taken from ref. 38.

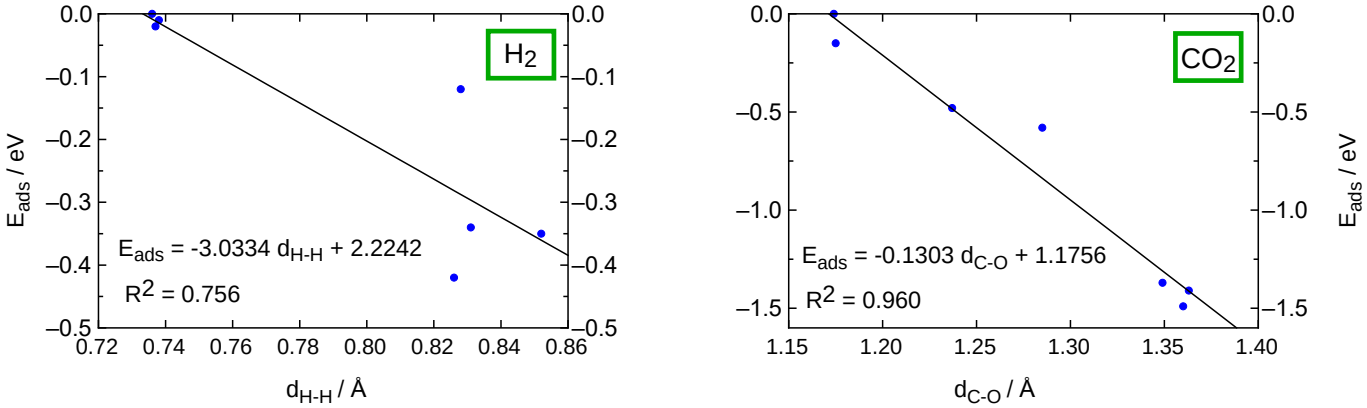

Figure 3. Correlation between the adsorption energies for H_2 (left) and CO_2 (right) and the H-H and C-O bond lengths, respectively.

REFERENCES

(1) Seneviratne, S. I.; Donat, M. G.; Pitman, A. J.; Knutti, R.; Wilby, R. L. Allowable CO2 Emissions Based on Regional and Impact-Related Climate Targets. *Nature* **2016**, *529* (7587), 477–483.

(2) Licker, R.; Ekwurzel, B.; Doney, S. C.; Cooley, S. R.; Lima, I. D.; Heede, R.; Frumhoff, P. C. Attributing Ocean Acidification to Major Carbon Producers. *Environ. Res. Lett.* **2019**, *14* (12), 124060.

(3) Barbir, F. Transition to Renewable Energy Systems with Hydrogen as an Energy Carrier☆. *Energy* **2009**, *34* (3), 308–312.

(4) Dincer, I. Renewable Energy and Sustainable Development: A Crucial Review. *Renew. Sust. Energ. Rev*, **2000**, *4* (2), 157–175.

(5) Jalama, K. Carbon Dioxide Hydrogenation over Nickel-, Ruthenium-, and Copper-Based Catalysts: Review of Kinetics and Mechanism. *Cataly. Rev.* **2017**, *59* (2), 95–164.

(6) Kattel, S.; Liu, P.; Chen, J. G. Tuning Selectivity of CO $_2$ Hydrogenation Reactions at the Metal/Oxide Interface. *J. Am. Chem. Soc.* **2017**, *139* (29), 9739–9754.

(7) Li, W.; Wang, H.; Jiang, X.; Zhu, J.; Liu, Z.; Guo, X.; Song, C. A Short Review of Recent Advances in CO_2 Hydrogenation to Hydrocarbons over Heterogeneous Catalysts. *RSC Adv.* **2018**, *8* (14), 7651–7669.

(8) Wang, W.; Wang, S.; Ma, X.; Gong, J. Recent Advances in Catalytic Hydrogenation of Carbon Dioxide. *Chem. Soc. Rev.* **2011**, *40* (7), 3703.

(9) J. M. Thomas and W. J. Thomas, Principles and Practice of Heterogeneous Catalysis, VCH, Weinheim, 1997.

(10) Chang, F.-W.; Kuo, M.-S.; Tsay, M.-T.; Hsieh, M.-C. Hydrogenation of CO2 over Nickel Catalysts on Rice Husk Ash-Alumina Prepared by Incipient Wetness Impregnation. *Appl. Catal. A-Gen.* **2003**, *247* (2), 309–320.

(11) Aziz, M. A. A.; Jalil, A. A.; Triwahyono, S.; Mukti, R. R.; Taufiq-Yap, Y. H.; Sazegar, M. R. Highly Active Ni-Promoted Mesostructured Silica Nanoparticles for CO2 Methanation. *Appl. Catal. B-Environ*, **2014**, *147*, 359–368.

(12) Tada, S.; Shimizu, T.; Kameyama, H.; Haneda, T.; Kikuchi, R. Ni/CeO2 Catalysts with High CO2 Methanation Activity and High CH4 Selectivity at Low Temperatures. *Int. J. Hydrogen Ener.* **2012**, *37* (7), 5527–5531.

(13) Ocampo, F.; Louis, B.; Kiwi-Minsker, L.; Roger, A.-C. Effect of Ce/Zr Composition and Noble Metal Promotion on Nickel Based CexZr1−xO2 Catalysts for Carbon Dioxide Methanation. *Appl. Catal. A-Gen.* **2011**, *392* (1–2), 36–44.

(14) Zhou, G.; Liu, H.; Cui, K.; Xie, H.; Jiao, Z.; Zhang, G.; Xiong, K.; Zheng, X. Methanation of Carbon Dioxide over Ni/CeO 2 Catalysts: Effects of Support CeO 2 Structure. *Int. J. Hydrogen Ener.* **2017**, *42* (25), 16108–16117.

(15) Hwang, S.; Hong, U. G.; Lee, J.; Baik, J. H.; Koh, D. J.; Lim, H.; Song, I. K. Methanation of Carbon Dioxide Over Mesoporous Nickel–M–Alumina (M = Fe, Zr, Ni, Y, and Mg) Xerogel Catalysts: Effect of Second Metal. *Catal Lett* **2012**, *142* (7), 860–868.

(16) Yang, L.; Pastor-Pérez, L.; Gu, S.; Sepúlveda-Escribano, A.; Reina, T. R. Highly Efficient Ni/CeO2-Al_2O_3 Catalysts for CO_2 Upgrading via Reverse Water-Gas Shift: Effect of Selected Transition Metal Promoters. *Appl. Catal. B-Environ*, **2018**, *232*, 464–47.

(17) Sun, F.; Yan, C.; Wang, Z.; Guo, C.; Huang, S. Ni/Ce–Zr–O Catalyst for High CO_2 Conversion during Reverse Water Gas Shift Reaction (RWGS). *Int. J. Hydrogen Ener.* **2015**, *40* (46), 15985–15993.

(18) Rodriguez, J. A.; Liu, P.; Stacchiola, D. J.; Senanayake, S. D.; White, M. G.; Chen, J. G. Hydrogenation of CO_2 to Methanol: Importance of Metal–Oxide and Metal–Carbide Interfaces in the Activation of CO_2. *ACS Catal.* **2015**, *5* (11), 6696–6706.

(19) Vidal, A. B.; Feria, L.; Evans, J.; Takahashi, Y.; Liu, P.; Nakamura, K.; Illas, F.; Rodriguez, J. A. CO_2 Activation and Methanol Synthesis on Novel Au/TiC and Cu/TiC Catalysts. *J. Phys. Chem. Lett.* **2012**, *3* (16), 2275–2280.

(20) Rodriguez, J. A.; Evans, J.; Feria, L.; Vidal, A. B.; Liu, P.; Nakamura, K.; Illas, F. CO_2 Hydrogenation on Au/TiC, Cu/TiC, and Ni/TiC Catalysts: Production of CO, Methanol, and Methane. *J. Catal.* **2013**, *307*, 162–169.

(21) Rodriguez, J. A.; Illas, F. Activation of Noble Metals on Metal-Carbide Surfaces: Novel Catalysts for CO Oxidation, Desulfurization and Hydrogenation Reactions *Phys. Chem. Chem. Phys*., **2012**, 14, 427-438.

(22) Tauster, S. J. Strong Metal-Support Interactions. *Accounts Chem. Res.* **1987**, *20*, 6.

(23) Tauster, S. J.; Fung, S. C.; Garten, R. L. Strong Metal-Support Interactions. Group 8 Noble Metals Supported on Titanium Dioxide. *J. Am. Chem. Soc.* **1978**, *100* (1), 170–175.

(24) Tauster, S. J.; Fung, S. C.; Baker, R. T. K.; Horsley, J. A. Strong Interactions in Supported-Metal Catalysts. *Science* **1981**, *211* (4487), 1121–1125.

(25) van Deelen, T. W.; Hernández Mejía, C.; de Jong, K. P. Control of Metal-Support Interactions in Heterogeneous Catalysts to Enhance Activity and Selectivity. *Nat Catal.* **2019**, *2* (11), 955–970.

(26) Klyushin, A. Yu.; Jones, T. E.; Lunkenbein, T.; Kube, P.; Li, X.; Hävecker, M.; Knop-Gericke, A.; Schlögl, R. Strong Metal Support Interaction as a Key Factor of Au Activation in CO Oxidation. *ChemCatChem* **2018**, *10* (18), 3985–3989.

(27) Bruix, A.; Rodriguez, J. A.; Ramírez, P. J.; Senanayake, S. D.; Evans, J.; Park, J. B.; Stacchiola, D.; Liu, P.; Hrbek, J.; Illas, F. A New Type of Strong Metal–Support Interaction and the Production of H_2 through the Transformation of Water on Pt/CeO_2 (111) and Pt/CeO_x /TiO_2 (110) Catalysts. *J. Am. Chem. Soc.* **2012**, *134* (21), 8968–8974.

(28) Prats, H.; Posada-Pérez, S.; Rodriguez, J. A.; Sayós, R.; Illas, F. Kinetic Monte Carlo Simulations Unveil Synergic Effects at Work on Bifunctional Catalysts. *ACS Catal.* **2019**, *9* (10), 9117–9126

(29) Piñero, J. J.; Ramírez, P. J.; Bromley, S. T.; Illas, F.; Viñes, F.; Rodriguez, J. A. Diversity of Adsorbed Hydrogen on the TiC(001) Surface at High Coverages. *J. Phys. Chem. C* **2018**, 122 (49), 28013–28020.

(30) Lozano-Reis, P.; Sayós, R.; Rodriguez, J. A.; Illas, F. Structural, Electronic, and Magnetic Properties of Ni Nanoparticles Supported on the TiC(001) Surface. *Phys. Chem. Chem. Phys.* **2020**, *22* (45), 26145–26154

(31) Kresse, G.; Hafner, J. *Ab Initio* Molecular Dynamics for Liquid Metals. *Phys. Rev. B* **1993**, *47* (1), 558–561.

(32) Kresse, G.; Furthmüller, J. Efficient Iterative Schemes for *Ab Initio* Total-Energy Calculations Using a Plane-Wave Basis Set. *Phys. Rev. B* **1996**, *54* (16), 11169–11186.

(33) Kresse, G.; Furthmüller, J. Efficiency of Ab-Initio Total Energy Calculations for Metals and Semiconductors Using a Plane-Wave Basis Set. *Comp. Mater. Sci.* **1996**, *6* (1), 15–50.

(34) Kresse, G.; Joubert, D. From Ultrasoft Pseudopotentials to the Projector Augmented-Wave Method. *Phys. Rev. B* **1999**, *59* (3), 1758–1775.

(35) Wellendorff, J.; Lundgaard, K. T.; Møgelhøj, A.; Petzold, V.; Landis, D. D.; Nørskov, J. K.; Bligaard, T.; Jacobsen, K. W. Density Functionals for Surface Science: Exchange-Correlation Model Development with Bayesian Error Estimation. *Phys. Rev. B* **2012**, *85* (23), 235149.

(36) Wellendorff, J.; Silbaugh, T. L.; Garcia-Pintos, D.; Nørskov, J. K.; Bligaard, T.; Studt, F.; Campbell, C. T. A Benchmark Database for Adsorption Bond Energies to Transition Metal Surfaces and Comparison to Selected DFT Functionals. *Surf. Sci.* **2015**, *640*, 36–44.

(37) Campbell, C. T. Energies of Adsorbed Catalytic Intermediates on Transition Metal Surfaces: Calorimetric Measurements and Benchmarks for Theory. *Acc. Chem. Res.* **2019**, *52* (4), 984–993

(38) Lozano-Reis, P.; Prats, H.; Gamallo, P.; Illas, F.; Sayós, R. Multiscale Study of the Mechanism of Catalytic CO_2 Hydrogenation: Role of the Ni(111) Facets. *ACS Catal.* **2020**, *10* (15), 8077–8089.

(39) Zhai, H.; Alexandrova, A. N. Local Fluxionality of Surface-Deposited Cluster Catalysts: The Case of Pt_7 on Al_2O_3. *J. Phys. Chem. Lett.* **2018**, *9* (7), 1696–1702.

(40) Sun, G.; Fuller, J. T.; Alexandrova, A. N.; Sautet, P. Global Activity Search Uncovers Reaction Induced Concomitant Catalyst Restructuring for Alkane Dissociation on Model Pt Catalysts. *ACS Catal.* **2021**, *11* (3), 1877–1885.

(40) Monkhorst, H. J.; Pack, J. D. Special Points for Brillouin-Zone Integrations. *Phys. Rev. B* **1976**, *13* (12), 5188–5192.

(42) Jónsson, H.; Mills, G.; Jacobsen, K. W. Nudged Elastic Band Method for Finding Minimum Energy Paths of Transitions. In *Classical and Quantum Dynamics in Condensed Phase Simulations*; WORLD SCIENTIFIC: LERICI, Villa Marigola, 1998; pp 385–404.

(43) Henkelman, G.; Uberuaga, B. P.; Jónsson, H. A Climbing Image Nudged Elastic Band Method for Finding Saddle Points and Minimum Energy Paths. *J. Chem. Phys.* **2000**, *113* (22), 9901–9904.

(44) Smidstrup, S.; Pedersen, A.; Stokbro, K.; Jónsson, H. Improved Initial Guess for Minimum Energy Path Calculations. *J. Chem. Phys.* **2014**, *140* (21), 214106.

(45) Hjorth Larsen, A.; Jørgen Mortensen, J.; Blomqvist, J.; Castelli, I. E.; Christensen, R.; Dułak, M.; Friis, J.; Groves, M. N.; Hammer, B.; Hargus, C.; Hermes, E. D.; Jennings, P. C.; Bjerre Jensen, P.; Kermode, J.; Kitchin, J. R.; Leonhard Kolsbjerg, E.; Kubal, J.; Kaasbjerg, K.; Lysgaard, S.; Bergmann Maronsson, J.; Maxson, T.; Olsen, T.; Pastewka, L.; Peterson, A.; Rostgaard, C.; Schiøtz, J.; Schütt, O.; Strange, M.; Thygesen, K. S.; Vegge, T.; Vilhelmsen, L.; Walter, M.; Zeng, Z.; Jacobsen, K. W. The Atomic Simulation Environment—a Python Library for Working with Atoms. *J. Phys.: Condens. Matter* **2017**, *29* (27), 273002.

(46) Liu, X.; Sun, L.; Deng, W.-Q. Theoretical Investigation of CO_2 Adsorption and Dissociation on Low Index Surfaces of Transition Metals. *J. Phys. Chem. C* **2018**, 122 (15), 8306–8314.

(47) Freund, H.-J.; Roberts, M. W. Surface Chemistry of Carbon Dioxide. *Surf. Sci. Rep.* **1996**, 25 (8), 225–273.

(48) Kunkel, C.; Viñes, F.; Illas, F. Transition Metal Carbides as Novel Materials for CO_2 Capture, Storage, and Activation Energy. *Environ. Sci.* **2016**, 9, 141-144.

(49) López, M.; Broderick, L.; Carey, J. J.; Viñes, F.; Nolan, M.; Illas, F. Tuning Transition Metal Carbide Activity by Surface Metal Alloying: A Case Study on CO_2 Capture and Activation. *Phys. Chem. Chem. Phys.* **2018**, *20* (34), 22179–22186.

(50) López, M.; Viñes, F.; Nolan, M.; Illas, F. Predicting the Effect of Dopants on CO_2 Adsorption in Transition Metal Carbides: Case Study on TiC (001). *J. Phys. Chem. C* **2020**, *124* (29), 15969–15976.

(51) Posada-Pérez, S.; Viñes, F.; Rodríguez, J. A.; Illas, F. Structure and electronic properties of Cu nanoclusters supported on Mo_2C(001) and MoC(001) surfaces. *J. Chem. Phys*. **2015**, 143, 114704.

(52) He, Y.; Wang, W. H_2 Dissociation on H-Precovered Ni(100) Surface: Physisorbed State and Coverage Dependence. *J. Phys. Chem. C* **2019**, *123*, 5365-5377.

(53) Florez, E.; Gomez, T.; Liu, P.; Rodriguez, J. A.; Illas, F. Hydrogenation Reactions on Au/TiC(001): Effects of Au↔C Interactions on the Dissociation of H_2. *ChemCatChem* **2010**, *2* (10), 1219–1222.

(54)Gomez, T.; Florez, E.; Rodriguez, J. A.; Illas, F. Reactivity of Transition Metals (Pd, Pt, Cu, Ag, Au) toward Molecular Hydrogen Dissociation: Extended Surfaces versus Particles Supported on TiC(001) or Small Is Not Always Better and Large Is Not Always Bad. *J. Phys. Chem. C* **2011**, *115* (23), 11666–11672.

(55) Prats, H.; Piñero, J. J.; Viñes, F.; Bromley, S. T.; Sayós, R.; Illas, F. Assessing the Usefulness of Transition Metal Carbides for Hydrogenation Reactions. *Chem. Commun.* **2019**, *55* (85), 12797–12800.